Mass transfer rate effects on the cavitating vortex shedding flow around a circular cylinder at low Reynolds number

C Jian, E Xavier *
Barcelona Fluids & Energy Lab, Universitat Politècnica de Catalunya, Av. Diagonal 647, 08028 Barcelona, Spain

E-mail: xavier.escaler@upc.edu

Abstract. Cavitating vortex shedding is a flow phenomenon commonly encountered behind bluff bodies in hydraulic machinery and systems and the generated vapor bubbles significantly change the dynamic behavior of the vortices. In addition, the collapses of the cavities become a source of unwanted effects such as vibration, noise and material erosion. In this study, the numerical results of the cavitating vortex shedding behind a circular cylinder at low Reynolds number have been compared and analyzed using different mass transfer rate values between the vapor and the liquid water phases. For that, the transport equation for the vapor volume fraction coupled with the explicit source term based on the simplification of the Rayleigh-Plesset equation has been solved. Commonly, this explicit source term that accounts for the mass transfer rate is driven by a function of the pressure difference, the vapor volume fraction and several empirical factors. To understand the effects of this rate, its value has been gradually increased from its default value up to the infinite when the equilibrium assumption for the barotropic flow is satisfied. The obtained results show that as the rate is increased, higher gradients of the vapor volume fraction and of the pressure near the interface between the vapor and the liquid phases are predicted. However, the frequency of the vortex shedding is slightly affected by the increase of the mass transfer rate.

1. Introduction

The cavitating vortex shedding behind a circular cylinder is one of the most canonical cases encountered in the hydraulic systems. When the vaporous cavities appear, the dynamic behavior of the vortices tends to change dramatically. Nowadays, the numerical methods have become a reliable and efficient tool to analyze and predict this complex dynamic behavior.

To numerically simulate such cavitating flows, two different assumptions are taken for the mass transfer between the liquid and the vapor: (i) the equilibrium flow assumption, which defines the pressure-density trajectory following a unique barotropic law [1]; (ii) the finite mass transfer rate assumption, which can be realized by the additional vapor volume fraction equation with a finite mass transfer source term [2]. And the difference between the two assumptions tends to be mimicked if the finite mass transfer rate increases to the infinity [1]. Schenke et al [3] also pointed out that the equilibrium assumption can be realized by

multiplying the finite source term and the pressure time derivative. Through numerical transient results of the Rayleigh bubble collapse with different condensation rates, they concluded that a lower condensation rate tends to drive the inertial flow across the condensation interface, while a higher condensation rate tends to lead the condensation interface move ahead of the inertial flow. Besides the condensation rate, the vaporization rate is also an important factor for the simulation of cavitation. Most of the research suggests that a higher value of the vaporization rate produces more accurate results, for example, the work of Ghahramani et al [4] showed that the vaporization rate coefficient should be "as high as possible without compromising numerical stability".

However, until now, the selection of the finite mass transfer rates has mainly relied on the researchers' experience. Therefore, in the current study, we have firstly derived the criteria to estimate the possible limits of the time step and of the vaporization and condensation empirical coefficients in the finite mass transfer rate cavitation model, for instance, the Zwart-Gerber-Belamri (ZGB) cavitation model. Then, the cavitating vortex shedding behind a circular cylinder has been used as a canonical case to compare numerically the effects of selecting different mass transfer rate conditions. Base on the results, we have investigated the effects of the mass transfer rate on the dynamic behavior of cavitating vortex shedding flows as well as on the unsteady pressure field.

2. Methodology and validation

2. 1 The criteria of finite mass transfer rate cavitation model

As previously mentioned, the selection of the finite mass transfer rate or the corresponding empirical coefficient lacks clear recommendations based on experimental and numerical evidence. Until now, none criteria or specific guide is available for the selection of these coefficients. Following the idea of Schenke et al [3], the equilibrium flow assumption, in which the finite mass transfer rate tends to infinity, has been considered in order to derive a criteria for selecting these coefficients and/or the time step size for the numerical simulation of cavitation vortex shedding.

The vapor volume fraction transport equation accounting for the finite mass transfer rate is expressed as:

$$\frac{\partial(\rho_V \alpha)}{\partial t} + \frac{\partial(\rho_V \alpha u_i)}{\partial x_i} = \dot{R} \quad \text{or} \quad \frac{\partial \alpha}{\partial t} + \frac{\partial(\alpha u_i)}{\partial x_i} = \frac{\dot{R}}{\rho_V} \tag{1}$$

where α is the vapor volume fraction; the ρ_V is the vapor density and the mass transfer source term $\dot{R}$ accounts for the mass transfer rate between the liquid and vapor.

The mixture density is given by $\rho = \rho_V \alpha + \rho_L(1-\alpha)$, where the ρ_L is the liquid density. Thus the mass conservation equation can be expressed as:

$$\frac{\partial(\rho)}{\partial t} + \frac{\partial(\rho u_i)}{\partial x_i} = 0 \tag{2}$$

Combining equations (1) and (2), the following expression is established:

$$\frac{\mathrm{d}\alpha}{\mathrm{d}t} = \frac{\rho}{\rho_V \rho_L} \dot{R} \tag{3}$$

For the equilibrium flow assumption, the time derivative $\left|\frac{\mathrm{d}\alpha}{\mathrm{d}t}\right|$ satisfies:

$$\left|\frac{\mathrm{d}\alpha}{\mathrm{d}t}\right| = \left|\frac{1}{dt}\right| \tag{4}$$

While for the finite mass transfer rate assumption, the time derivative $\left|\frac{\mathrm{d}\alpha}{\mathrm{d}t}\right|$ is controlled by the following condition:

$$\left|\frac{\mathrm{d}\alpha}{\mathrm{d}t}\right| \leq \left|\frac{1}{dt}\right| \tag{5}$$

Here, $\dot{R}$ is modelled by the Zwart-Gerber-Belamri cavitation model:

$$\dot{R} = \begin{cases} F_{cond}\frac{3\alpha\rho_V}{R_B}\sqrt{\frac{2}{3}\frac{(p-p_V)}{\rho_L}}, p > p_V \\ -F_{vap}\frac{3\rho_V(1-\alpha)\alpha_{nuc}}{R_B}\sqrt{\frac{2}{3}\frac{(p_V-p)}{\rho_L}}, p < p_V \end{cases} \tag{6}$$

where p_{V} is the saturated vapor pressure and equal to 2340 Pa, R_B is the bubble radius equal to 10^{-6} m, α_{nuc} is the nucleation site of the volume fraction equal to 5×10^{-4}, and the default empirical condensation and vaporization coefficients, F_{cond} and F_{vap}, are equal to 0.01 and 50.0, respectively.

Assuming that the minimal pressure p is equal to 0 (note that any value below 0 is non-physical) and that the vapor volume fraction is in the interval $[0,1]$ and substituting F_{vap} from equation (3) into the inequality equation (5) we obtain:

$$\left|\frac{\mathrm{d}\alpha}{\mathrm{d}t}\right| = \frac{\rho}{\rho_L}F_{vap}\frac{3(1-\alpha)\alpha_{nuc}}{R_B}\sqrt{\frac{2}{3}\frac{(p_V)}{\rho_L}} \leq \left|\frac{1}{dt}\right| \tag{7}$$

Therefore, the condition for F_{vap} is governed by:

$$\left|\frac{\rho}{\rho_L}F_{vap}\frac{3(1-\alpha)\alpha_{nuc}}{R_B}\sqrt{\frac{2}{3}\frac{(p_V)}{\rho_L}}\right| dt \leq 1 \tag{8}$$

Meanwhile, for the given F_{vap}, the time step, dt, satisfies the following condition:

$$dt \leq 1\Big/\left|\frac{\rho}{\rho_L}F_{vap}\frac{3(1-\alpha)\alpha_{\mathrm{nuc}}}{R_B}\sqrt{\frac{2}{3}\frac{(p_{\mathrm{V}})}{\rho_L}}\right| \tag{9.a}$$

Furthermore, for the given dt, F_{vap} satisfies the following criteria:

$$\frac{\rho}{\rho_L}F_{vap}\frac{3(1-\alpha)\alpha_{\mathrm{nuc}}}{R_B}\sqrt{\frac{2}{3}\frac{(p_{\mathrm{V}})}{\rho_L}} \leq \left|\frac{1}{dt}\right| \quad \text{or} \quad F_{vap} \leq \left|\frac{1}{dt}\right|\Big/\left\{\frac{\rho}{\rho_L}\frac{3(1-\alpha)\alpha_{\mathrm{nuc}}}{R_B}\sqrt{\frac{2}{3}\frac{(p_{\mathrm{V}})}{\rho_L}}\right\} \tag{9.b}$$

Similarly, the local pressure, p, can be written as:

$$\frac{(p-p_{\mathrm{V}})}{\rho_L} = \frac{1}{2}\sigma_{local}{U_{ref}}^2 \tag{10}$$

where $\sigma_{local} = \frac{(p-p_{\mathrm{V}})}{\frac{1}{2}\rho_L{U_{ref}}^2}$.

Thus, the constrains for the condensation rate are controlled by:

$$dt \leq 1\Big/\left|\frac{\rho}{\rho_L}F_{cond}\frac{3\alpha}{R_B}\sqrt{\frac{1}{3}\sigma_{local}}U_{ref}\right| \tag{11.a}$$

$$F_{cond} \leq \left|\frac{1}{dt}\right|\Big/\left\{\frac{\rho}{\rho_L}\frac{3\alpha}{R_B}\sqrt{\frac{1}{3}\sigma_{local}}U_{ref}\right\} \tag{11.b}$$

In conclusion, the dt for simulating the mass transfer rate with the Zwart-Gerber-Belamri cavitation model should satisfy the following condition:

$$dt \leq \mathrm{Min}\left(1\Big/\left|\frac{\rho}{\rho_L}F_{vap}\frac{3(1-\alpha)\alpha_{\mathrm{nuc}}}{R_B}\sqrt{\frac{2}{3}\frac{(p_{\mathrm{V}})}{\rho_L}}\right|, 1\Big/\left|\frac{\rho}{\rho_L}F_{cond}\frac{3\alpha}{R_B}\sqrt{\frac{1}{3}\sigma_{local}}U_{ref}\right|\right) \tag{12}$$

Also, F_{vap}, and F_{cond} should meet the following conditions:

$$\begin{cases} F_{vap} \leq \left|\frac{1}{dt}\right| \Big/ \left\{\frac{\rho}{\rho_L}\frac{3(1-\alpha)\alpha_{\text{nuc}}}{R_B}\sqrt{\frac{2}{3}\frac{(p_V)}{\rho_L}}\right\} \\ F_{cond} \leq \left|\frac{1}{dt}\right| \Big/ \left\{\frac{\rho}{\rho_L}\frac{3\alpha}{R_B}\sqrt{\frac{1}{3}\sigma_{local}U_{ref}}\right\} \end{cases} \tag{13}$$

Equations (12) and (13) show that there is strong link between the time step, dt, and the mass transfer rates that depend on the vaporization and condensation coefficients, F_{vap} and F_{cond}. Regardless of the local pressure, p, the upper limit of dt is inversely proportional to the mass transfer rate. While, for a given dt, F_{vap} and F_{cond} are also limited by the inverse value of dt. So, these expressions can be used to select an adequate combination of dt, F_{vap} and F_{cond} for the numerical simulation of cavitation. It should be noticed that the minimum value of p can dramatically change the relationship among these variables. If the minimum value of p is close to the vapor pressure, p_V, the upper limit of F_{vap} can increase to the infinity which corresponds to the equilibrium assumption. However, such strong volume fraction variation provoked by a very tiny pressure change may tend to induce numerical instabilities. Therefore, the determination of the minimum p allowed in the simulations still needs further investigations.

2. 2 Mesh topology and numerical setup

A two-dimensional computational domain has been used as shown in figure 1a. We have placed a circular cylinder with diameter D as the cavitating source in the center of the circular computational domain with diameter 100D. Details of the structured mesh close to the circular cylinder surface with different resolutions are shown in Figure 1b, 1c and 1d. A uniform inflow with $U_{ref} = 10\ \text{m/s}$ has been set at the inlet boundary to guarantee a Reynolds number, $\text{Re} = U_{ref}D/\upsilon$, equal to 200. A static pressure boundary condition , p_{ref}, has been applied at the outlet surface based on the corresponding cavitation number, $\sigma = \frac{(p_{ref}-p_V)}{\frac{1}{2}\rho_L {U_{ref}}^2}$. Besides the aforementioned mixture mass conservation equation and the vapor volume fraction transport equation, the laminar model has been used for solving the flow field.

After the physical model and boundary conditions are established, the governed equations are discretized to obtained the numerical solution of the cavitating vortex shedding flow. In spatial discretization, the second-order upwind scheme has been applied to approximate the flux of the flow quantities. In temporal discretization, the second-order implicit scheme has been used.

2. 3 Validation of single phase numerical results

To validate the unsteady results of a single phase flow obtained from the numerical setup, the Strouhal number, $St = fD/U_{ref}$ has been used, where f is the vortex shedding frequency. For that, the St calculated with the aforementioned three meshes with different refinement levels have been compared with those values obtained by Seo et al [5] to assess the sensitivity of the mesh resolution. As shown in table 1, the deviation between the numerical results and the referred results is about 2.1 % when the fine mesh is used. The sensitivity to the size of the time step on the transient numerical results has also been evaluated. In table 2, the St obtained with different time steps are presented and compared with the reference values. It can be seen that the deviation between the numerical results and the referred one increases with the decrease of the time step size. However, the differences among all the considered time step sizes are negligible.

Therefore, to guarantee a good balance between the numerical convergence requirements and the computational cost, a time step of 10^{-7}s has been used in the present work.

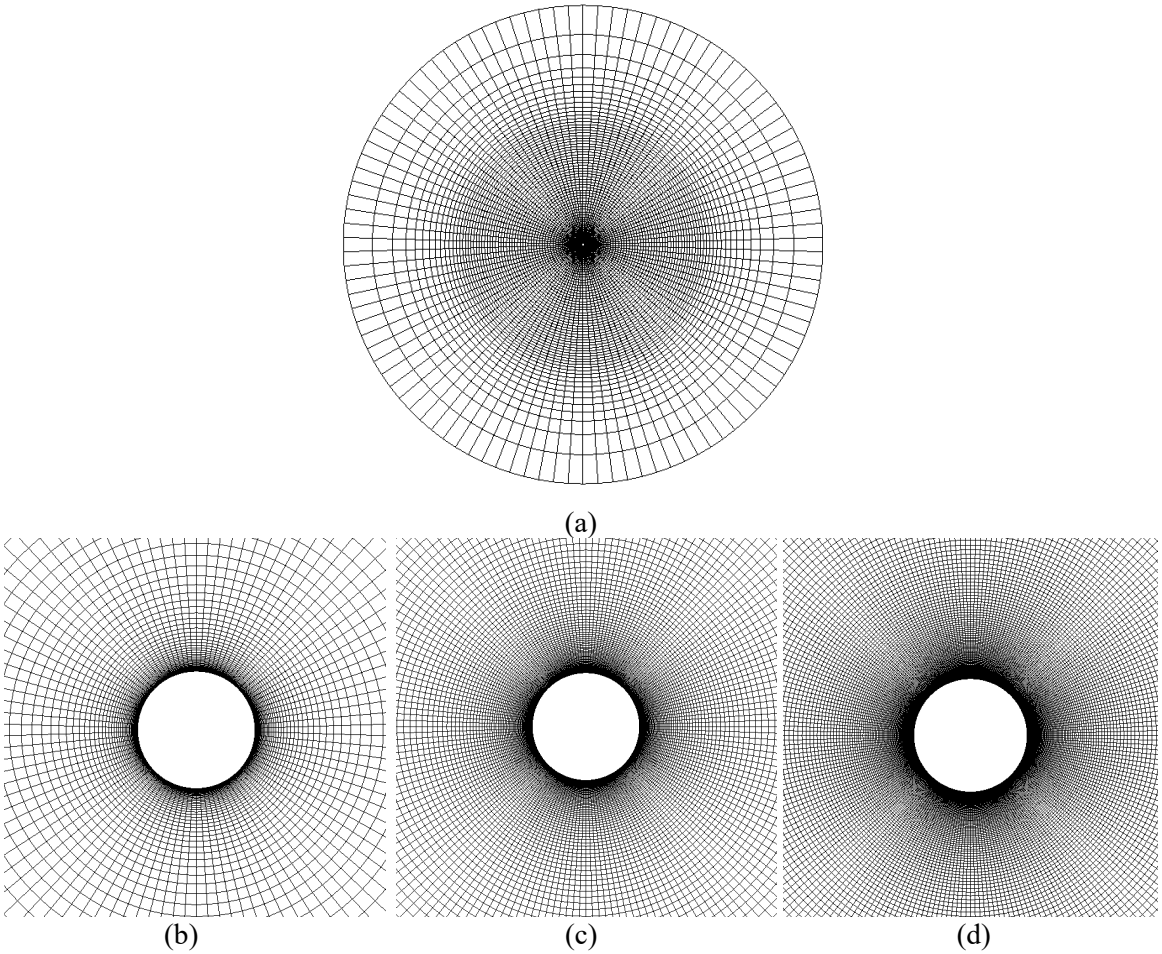

Figure 1. Complete computational domain (a) and zooms around the cylinder surface for the coarse mesh (b); the medium mesh (c) and the fine mesh (d).

Table 1. Sensitivity of the mesh resolution on the transient numerical results.

Mesh	St_{num}	St_{ref} from Seo et al [5]	Deviation (%)
Coarse	0.377		0.7
Medium	0.386	0.380	1.6
Fine	0.388		2.1

Table 2. Sensitivity of the time step on the transient numerical results

Time step [10^{-7}s]	St_{num}	St_{exp} from Seo et al [5]	Deviation [%]
2	0.385		1.3
1	0.388	0.380	2.1
0.5	0.389		2.4

3. Results and discussion

As aforementioned in section 2, it has been concluded that the selection of the ZGB cavitation mass transfer rate is dependent on the time step. The constants R_B and α_{nuc} have been taken with their default values and from equations (12) and (13) the following conditions are obtained that permit to specify the time step duration and the ZGB vaporization and condensation empirical coefficients:

$$dt \leq \text{Min}\left(1/\left|2\cdot 10^3 F_{vap}\right|, 1/\left|8\cdot 10^5 F_{cond}\sqrt{\tfrac{1}{3}\sigma_{local}}U_{ref}\right|\right) \tag{14}$$

Here, taken for simplicity $\sigma_{local} = 3$, then:

$$\begin{cases} F_{vap} \leq \left|\frac{1}{dt}\right| / \{2\cdot 10^3\} \\ F_{cond} \leq \left|\frac{1}{dt}\right| / \{8\cdot 10^5 U_{ref}\} \end{cases} \tag{15}$$

and, for $dt = 10^{-7}$s, Equation 15 gives the limits to select F_{vap} and F_{cond}:

$$F_{vap} \leq 5\cdot 10^3;\ F_{cond} \leq 1 \tag{16}$$

3. 1 Effect of the mass transfer rate on the vortex shedding dynamic behavior

Here, the dynamic behavior of cavitating vortex shedding behind the circular cylinder for different values of F_{vap} are compared. In table 3, it can be observed that, the obtained Strouhal number St, decreases as the vaporization coefficient F_{vap} increases. Also, figures 2 and 3 present the time history of the lift, C_L, and drag, C_D, coefficients for flow conditions at cavitation number $\sigma = 1.0$. As expected, the results indicate that the forces acting on the surface of the circular cylinder increase significantly as F_{vap} decreases.

When F_{vap} is equal to 5000, which corresponds to the maximum value indicated by the condition in equation (16), the dynamic behavior of the cavitating vortex shedding has been compared for different values of F_{cond} as well. The time histories of C_L and C_D at $\sigma = 1.0$ are presented in figures 4 and 5 where it can be seen that the maximum forces acting on the surface of the circular cylinder increase as F_{cond} increases. Meanwhile, as shown in table 6, it is observed that the higher values of F_{cond} provoke an increase of St.

At $F_{cond} = 1.0$, it is noted that an impulsive force exist both in the time history of C_L and C_D. The occurrence of this impulsive force is due to the pressure pulse provoked by the collapse of a vapor cavity inside the wake of the vortex. Therefore, the generation mechanism of the pressure pulse will be further discussed in the next section.

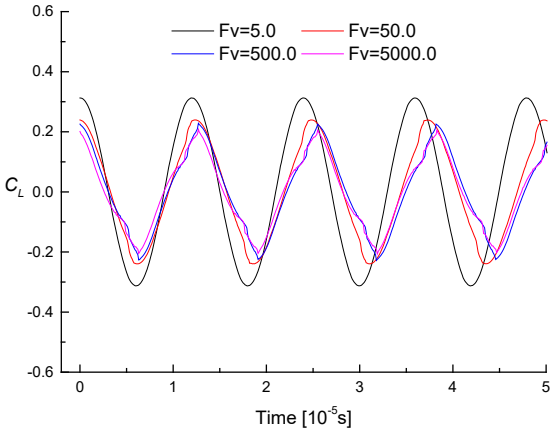

Figure 2. C_L evolution for different F_{vap}.

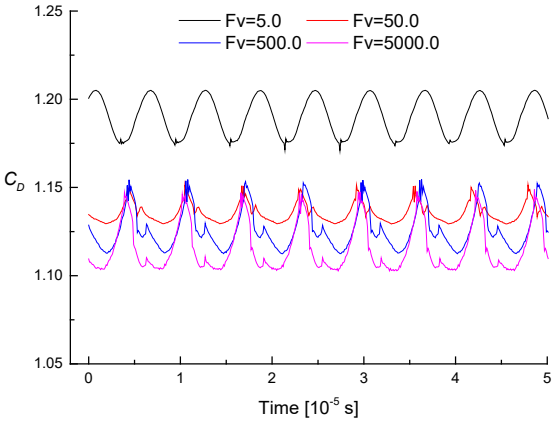

Figure 3. C_D evolution for different F_{vap}.

Table 3 Effect of the vaporization rate on the St value.

F_{vap}	F_{cond}	St_{num}	St_{ref} from Seo et al [5]	Deviation [%]
5	0.001	0.335	0.320	4.7
50	0.001	0.321		0.3
500	0.001	0.315		1.6
5000	0.001	0.313		2.2

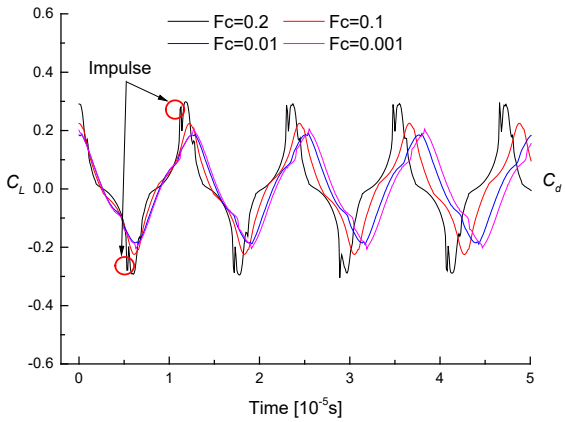

Figure 4. C_L evolution for different F_{cond}.

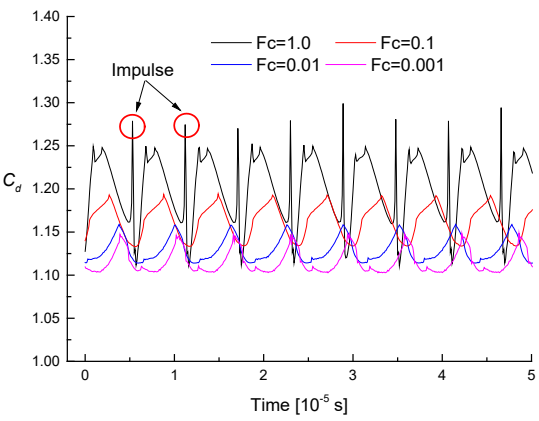

Figure 5. C_D evolution for different F_{cond}.

Table 4. Effect of condensation rate on St.

F_{vap}	F_{cond}	St_{num}	St_{ref} from Seo et al [5]	Deviation [%]
5000	0.001	0.313	0.320	2.2
5000	0.01	0.314		1.9
5000	0.1	0.328		2.5
5000	1	0.339		5.9

3. 2 Effect of mass transfer rate on the pressure field

The extreme levels of the pressure field obtained with the numerical solvers deserve to be analyzed. Most commercial solvers take the minimum absolute pressure value within the cavitation flow equal to the vapor pressure by default. The consequence of clipping the absolute pressure filed is that some results may be misinterpreted. To overcome this problem, the evolution of the minimum and maximum values of the non-clipped absolute pressure have been investigated in relation to the mass transfer rate and these values for different F_{vap} have been plotted in figure 6. It can be noted that the minimum local pressure increases as F_{vap} increases while the maximum local pressure is kept almost constant as F_{vap} increases. It can also be seen that nonphysical negative absolute pressures are only obtained for $F_{vap} = 5000$ when the minimum local pressure is above 0.

In figure 7, the pressure and vapor fraction have been plotted at the instant when the minimum pressure occurs that is located nearby the cavitation inception area and marked with a blue dot. This position seems not to change with the variation of F_{vap}. The increase of forces acting on the cylinder surface due to the decrease of F_{vap} can be explained by the fact that more negative pressure values are predicted for smaller values of of F_{vap}.

The effects of F_{cond} on the extreme values of the pressure field have been investigated while maintaining the minimum pressure above 0 by forcing F_{vap} = 5000. The minimum and maximum values of the absolute pressure at different F_{cond} values have been plotted in Figure 8. It is observed that the minimum local pressure slightly decreases as F_{cond} increases while the maximum local pressure slightly increases as F_{cond} increases and that its value is almost equal to the reference pressure p_{ref} if F_{cond} is smaller than 0.1. Then, a sharp growth of the maximum local pressure is produced at F_{cond} = 1.0.

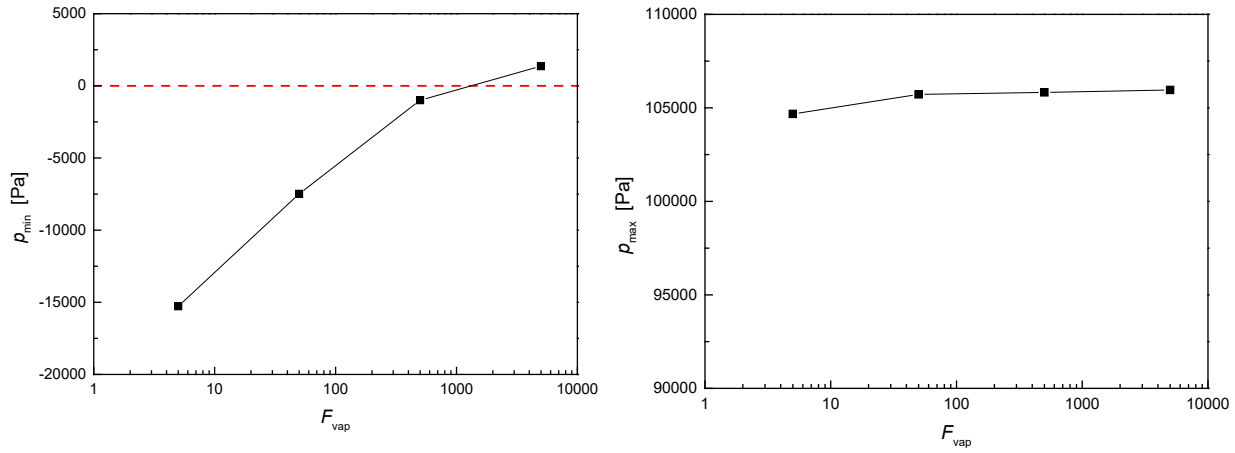

(a) (b)

Figure 6. Minimum (a) and maximum (b) values of the local pressure for different F_{vap}.

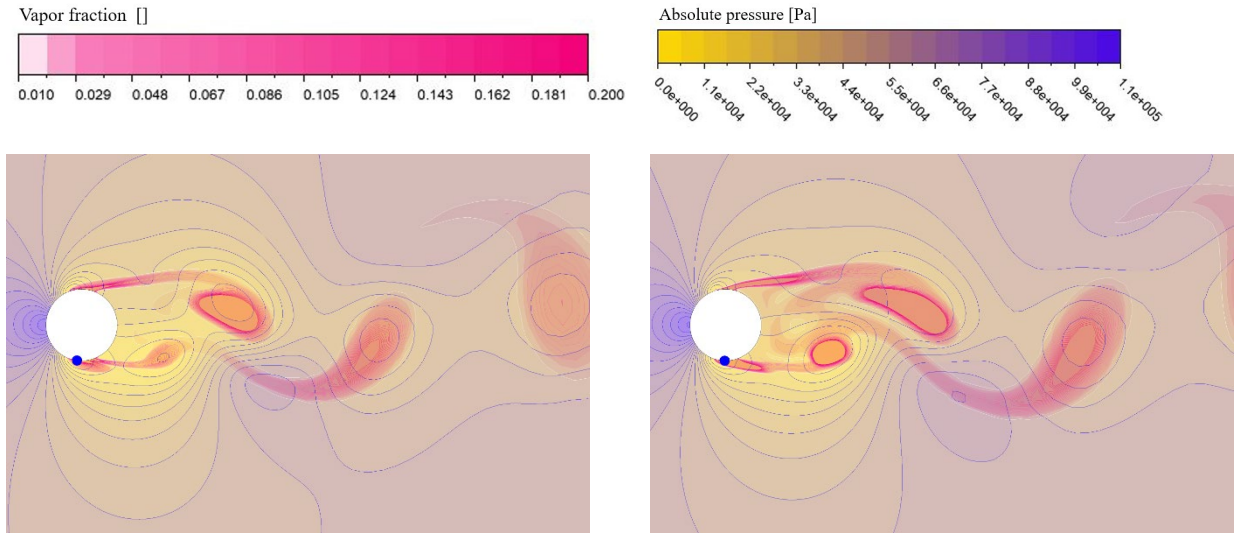

(a) $F_{vap} = 50\ F_{cond} = 0.001$ (b) $F_{vap} = 5000\ F_{cond} = 0.001$

Figure 7. Absolute pressure and vapor fraction for different F_{vap}.

In figure 9, the contours of the pressure and vapor volume fraction at F_{cond} equal to 0.1 and 1.0 are compared. The local maximum pressure, marked with a red dot, is located at two different positions. For

F_{cond} = 0.1, it is located at the stagnation point in front of the cylinder surface. However, at F_{cond}=1.0 the maximum value is located inside the collapsing vapor vortex. Furthermore, a shock wave pattern is observed around the collapsing cavity suggesting that the large condensation rate causes a dramatic local pressure rise similar to the expected behavior after a cavity collapse. However, to determine the physical meaning of this pressure impulse for the high condensation rate requires a further study.

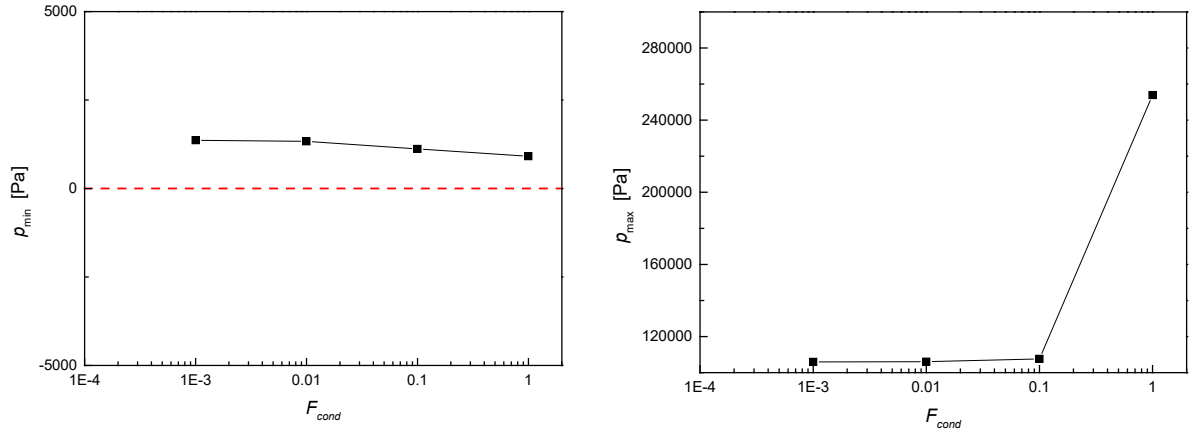

(a) (b)

Figure 8. Minimum (a) and maximum (b) of the local pressure for different F_{cond}.

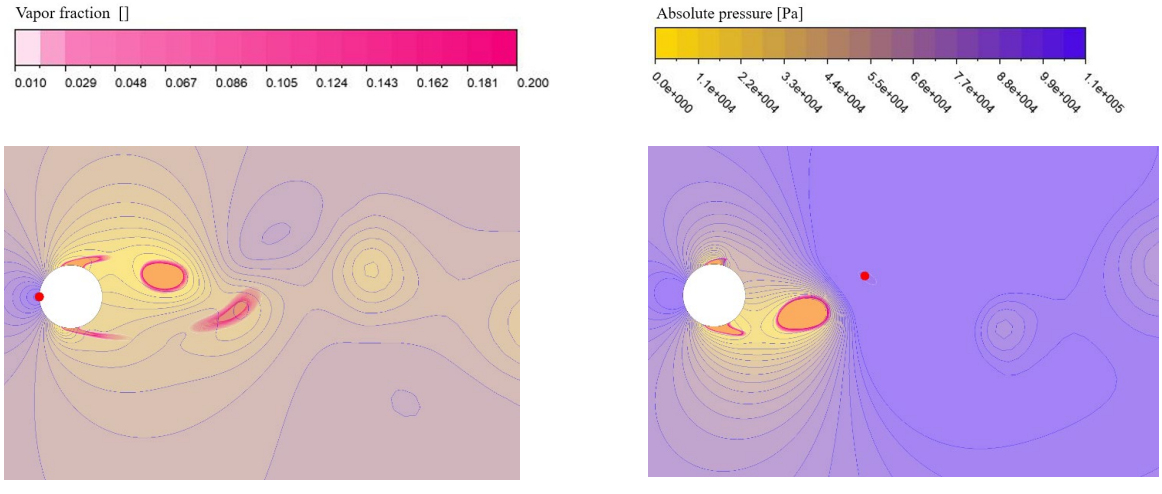

(a) $F_{vap} = 5000\ F_{cond} = 0.1$ (b) $F_{vap} = 5000\ F_{cond} = 1.0$

Figure 9. Absolute pressure and vapor fraction for different F_{cond}.

4. Conclusions

To achieve the equilibrium flow assumption in cavitation simulations, it would be necessary to increase the mass transfer rate up to its upper limit. However, it can be demonstrated that the selection of the time step also imposes restrictions to the possible range of values for this rate. Therefore, a preliminary study has served to derive the limits of the vaporization and condensation mass transfer rates when the minimum absolute local pressure is assumed to be zero. Then, the dynamic behavior and the main properties of the canonical cavitating vortex shedding flow behind a circular cylinder have been numerically calculated and compared for different mass transfer rates. It has been found that the vortex shedding frequency tends to decrease as the vaporization coefficient F_{vap} increases. On the other hand, the increase of F_{cond} provokes an increase of vortex shedding frequency. By observing the non-clipped absolute pressure filed at different mass transfer rates, it has been confirmed that a high value of the vaporization rate can increase the minimum pressure of the flow up to the vapor pressure value and thus resemble more the expected physical cavitation flow behavior. Contrarily, the change of the vaporization rate has less influence on the predicted maximum pressure levels. Moreover, the maximum pressure is mainly influenced by the condensation rate and its value sharply increases for $F_{cond} = 1.0$ when a strong pressure rise is predicted at the instant when the vortex cavity collapse takes place. Meanwhile the minimum pressure value is less affected by the change of condensation rate.

5. Acknowledgements

This project has received funding from the European Union's Horizon 2020 research and innovation program under grant agreement No 814958, and from China Scholarship Council No 201808320237.

6. References

[1] Koukouvinis P, and Gavaises M 2015 *Proc. Int. Symp. on Cavitation（Switzerland）*
[2] Goncalves E, and Patella R F 2009 *Comput. Fluids*. **38** 9
[3] Schenke Sören, van Terwisga T 2015 *Proc. Num. Towing Tank Symp (France)*
[4] Ghahramani E, Ström H, and Bensow R E 2021 *J. Fluid Mech.* **2021** 922
[5] Seo J H, Moon Y J, and Shin B R 2008 *J. Comput. Phys.* **227** 13